

On the path from xylem hydraulic failure to downstream cell death

Marylou Mantova¹ , Hervé Cochard¹ , Régis Burlett² , Sylvain Delzon² , Andrew King³,
Celia M. Rodriguez-Dominguez⁴ , Mutez A. Ahmed^{5,6} , Santiago Trueba²  and José M. Torres-Ruiz¹ 

¹Université Clermont Auvergne, INRAE, PIAF, 63000 Clermont-Ferrand, France; ²Université Bordeaux, INRAE, BIOGECO, 33615 Pessac, France; ³Synchrotron SOLEIL, L'Orme des Merisiers, 91190 Gif-sur-Yvette cedex, France; ⁴Irrigation and Crop Ecophysiology Group, Instituto de Recursos Naturales y Agrobiología de Sevilla (IRNAS, CSIC), Avenida Reina Mercedes, 10, 41012 Sevilla, Spain; ⁵Chair of Soil Physics, Bayreuth Center of Ecology and Environmental Research (BayCEER), University of Bayreuth, 95440 Bayreuth, Germany; ⁶Department of Land, Air and Water Resources, University of California Davis, Davis, CA 95616, USA

Summary

Author for correspondence:
José M. Torres-Ruiz
Email: torresruizjm@gmail.com

Received: 6 July 2022
Accepted: 17 October 2022

New Phytologist (2022)
doi: 10.1111/nph.18578

Key words: cavitation, cell dehydration, drought, membrane leakage, relative water content.

- Xylem hydraulic failure (HF) has been identified as a ubiquitous factor in triggering drought-induced tree mortality through the damage induced by the progressive dehydration of plant living cells. However, fundamental evidence of the mechanistic link connecting xylem HF to cell death has not been identified yet. The main aim of this study was to evaluate, at the leaf level, the relationship between loss of hydraulic function due to cavitation and cell death under drought conditions and discern how this relationship varied across species with contrasting resistances to cavitation.
- Drought was induced by withholding water from potted seedlings, and their leaves were sampled to measure their relative water content (RWC) and cell mortality. Vulnerability curves to cavitation at the leaf level were constructed for each species.
- An increment in cavitation events occurrence precedes the onset of cell mortality. A variation in cells tolerance to dehydration was observed along with the resistance to cavitation.
- Overall, our results indicate that the onset of cellular mortality occurs at lower RWC than the one for cavitation indicating the role of cavitation in triggering cellular death. They also evidenced a critical RWC for cellular death varying across species with different cavitation resistance.

Introduction

In the context of the ongoing climate change, temperature and precipitation patterns are changing in many areas world-wide (IPCC, 2022). Consequently, the severity of drought episodes is increasing in several areas of the world and is expected to continue to do so in the near future (IPCC, 2022). Climate change which has already shown important consequences on tree survival and forest dieback is therefore expected to dramatically accelerate forest mortality as drought intensity increases (Allen *et al.*, 2010; McDowell *et al.*, 2022).

The mechanisms of tree mortality under drought conditions have been largely evaluated in the last decades, and many studies have shown that the impairment of the water transport system leads trees to death through hydraulic failure (HF) (Urli *et al.*, 2013; Salmon *et al.*, 2015; Hammond *et al.*, 2019; Mantova *et al.*, 2021). Hydraulic failure occurs under drought conditions when there is an accumulation of emboli within the sapwood past a threshold after which water transport is irrecoverable (McDowell *et al.*, 2022). Even though HF has been unequivocally considered as the predominant triggering mechanism for tree death by ecophysiologicals and modellers (Anderegg

et al., 2015; Sperry & Love, 2015; Adams *et al.*, 2017; Brodribb *et al.*, 2020; Lemaire *et al.*, 2021) and should provoke tree mortality by leading to cellular desiccation and death (McDowell *et al.*, 2008, 2022), recent studies have shown that the empirically defined percentage loss of conductance (PLC) thresholds for mortality (50% and 88% for conifers and angiosperms respectively) were not precise enough when aiming to predict cell, tissue and thus tree death under drought conditions (Hammond *et al.*, 2019; Mantova *et al.*, 2021, 2022). Indeed, recent observations have shown how trees could recover from water stress even beyond those PLC thresholds, that is *c.* 80% for conifers (Hammond *et al.*, 2019) and after almost full embolization for angiosperms (Mantova *et al.*, 2021), and could also present no evidence of tissue death until very high level of embolization (*i.e.* 90%) (Johnson *et al.*, 2022).

Despite McDowell *et al.* (2008, 2022) hypothesizing that HF provokes tree mortality by leading to complete desiccation and cellular death, the consequences of HF on cellular dehydration and cellular mortality *per se* remain largely unexplored. Indeed, even though the correlation between HF and tree mortality has been largely assessed in woody species (Brodribb & Cochard, 2009; Choat *et al.*, 2012; Barigah *et al.*, 2013; Urli

et al., 2013; Adams *et al.*, 2017; Hammond *et al.*, 2019; Mantova *et al.*, 2021), only a single recent study performed on tomato species, a nonwoody species, and integrating HF and cell mortality has shown that vascular network failure in leaves leads to tissue death (Brodrribb *et al.*, 2021). Thus, even if Brodrribb *et al.* (2021) have evinced a strong mechanistic foundation linking xylem network failure and leaf tissue death, it remains unknown, for woody species, whether cells start to die at the onset of xylem cavitation or whether there is a delay before encountering cell damage. In addition, the level of PLC at which cellular death occurs and how it varies across species with contrasting resistance to xylem cavitation remain unexplored.

The decrease in relative water content (RWC) at the organ level has been linked with cell membrane disruption and thus cellular death in many studies (Wang *et al.*, 2008; Chaturvedi *et al.*, 2014; Guadagno *et al.*, 2017). These advances at the cellular level have led to a renewed integrative framework linking the dysfunction of the water transport system (i.e. the xylem) and cellular mortality recognizing the relevance of RWC and the level of cell membrane damage as good candidate variables for predicting mortality (Mantova *et al.*, 2022). Relative water content is a valuable water status indicator of cell stress as it represents relative cell volume shrinkage, cell membrane tension and turgor (Zhu, 2016; Sack *et al.*, 2018; Martinez-Vilalta *et al.*, 2019; Sapes *et al.*, 2019). Also, RWC presents the advantage of being a metric to which cells respond directly and being a direct measurement of the dehydration state of plant organs. Some empirical evidence has shown that the leaf RWC at turgor loss point (TLP) was relatively high and constant across species compared with the leaf water potential at TLP (Bartlett *et al.*, 2012). Thus, RWC could serve as a potential candidate to define a dehydration threshold (inflection point) below which cells start to suffer from water stress (Martinez-Vilalta *et al.*, 2019), which would be of great help when assessing the dynamic of cavitation propagation and cellular death.

Apart from changes in fluorescence noticed following initial cavitation (Brodrribb *et al.*, 2021), leaves show conjoint changes in leaf colour and increases in the rate of leaf shrinkage (Johnson *et al.*, 2018), due to the rapid dehydration of the mesophyll downstream (Brodrribb *et al.*, 2021). The changes in leaf colour have been attributed to the loss of turgor and the collapse of the palisade cells, which decrease the distance between cells, thereby decreasing light transmittance (Brodrribb *et al.*, 2021). However, even though tissue dehydration should be associated with structural changes, particularly shrinkage, occurring at the tissue level (Johnson *et al.*, 2018; Lamacque *et al.*, 2020; Bourbia *et al.*, 2021) and could also be responsible for cellular death (Mantova *et al.*, 2022), it has not been described yet if cell mortality is a consequence of cell cavitation (Rajashekar & Lafta, 1996; Sakes *et al.*, 2016), collapse or cytorrhysis (Oertli, 1986).

Considering the actual need to understand the underlying processes connecting HF and cellular mortality (Mantova *et al.*, 2022; McDowell *et al.*, 2022), the main aims of this study are to (1) evaluate whether the water transport impairment through cavitation is the triggering factor causing cell death under drought conditions in woody species, (2) study whether

the relationship between cavitation occurrence and cell death varies across species with contrasting resistances to drought and (3) identify a RWC threshold inducing plant cell damage from drought. We worked at the leaf level to elucidate the causal link between a decreasing water supply, caused by xylem cavitation, the decrease in leaf RWC (RWC_{Leaf}) and cell mortality. For this, we investigated three different species having contrasted cavitation resistance: *Eucalyptus viminalis*, *Laurus nobilis* and *Populus tremula* × *alba*. We exposed individuals of each species to severe drought conditions, and, during the dehydration process, we monitored their water status via the measurement of the leaf water potential (Ψ_{Leaf}) and RWC_{Leaf} . During leaf dehydration, we assessed cell vitality using the electrolyte leakage (EL) approach. We also performed synchrotron-based micro-CT to anatomically visualize the consequences of a decreasing water supply on the different leaf tissues and decipher the sequence of events leading to cell death. This approach gave us the opportunity to test the connection between cavitation and cell death in leaves.

Materials and Methods

Plant material and experimental setup

The experiments were carried out in three tree species: *E. viminalis* Labill., *L. nobilis* L. and *P. tremula* × *alba* (clone INRA 717-1B4), from February to September 2020. For each species, trees were grown under nonlimiting water conditions in 9.2, 7.5 and 4 l pots, respectively, at the INRAe PIAF Research Station of Clermont-Ferrand, France (45°46'10.793"N, 3°8'48.347"E) for *E. viminalis* and *P. tremula* × *alba* and in Les Chères, France (45°54'48.6"N, 4°39'14.399"E) for *L. nobilis*. *Eucalyptus viminalis* trees were 3 yr old at the time of the experiment, while *L. nobilis* individuals were 2 yr old and *P. tremula* × *alba* trees were 6 months old. For each species, between 6 and 11 plants were exposed to a progressive and total bench dehydration by withholding irrigation.

Leaf physiological traits

Pressure–volume curves Pressure–volume (PV) curves provide information about turgor pressure, osmotic pressure and elastic properties of cells and how these parameters change with cell water content during water stress. Pressure–volume curves were produced on six leaves per species, and TLP (expressed in MPa: Ψ_{TLP} or in the percentage of RWC: RWC_{TLP}) and modulus of elasticity (ϵ) were determined according to standard methods for each species (Sack *et al.*, 2010). Briefly, leaves were rehydrated overnight by soaking the leaf petiole in distilled water. Ψ_{Leaf} was measured with a Scholander-type pressure chamber (PMS, Corvallis, OR, USA), following precautions and recommendations by Rodriguez-Dominguez *et al.* (2022), while the weight was measured with a balance (Mettler AE 260, DeltaRange®; Mettler Toledo, Columbus, OH, USA) along the course of the experiment (13–15 times a day). The leaf dry mass was determined after drying the leaves at 70°C for 3 d.

Vulnerability curves to cavitation Leaf vulnerability to cavitation was assessed using the optical method (Brodrribb *et al.*, 2016) in six to eight intact and unpotted trees per species. Based on the principle that light interacts differently with the xylem that is water-filled or air-filled, it is possible to compare the quantitative differences in brightness caused by cavitation events between consecutive images and generate vulnerability curves over the decreasing water potential. Briefly, two healthy and fully expanded leaves per individual and species were installed on a scanner (V800 perfection; Epson, Suwa, Nagano, Japan), for *E. viminalis*, or on clamps equipped with a camera (<http://www.opensourceov.org/>), for *L. nobilis* and *P. tremula* × *alba*, and images were taken, using transmitted light to illuminate them, every 5 min during the dehydration process. The imaged area encompassed all vein orders, including the midrib. Scan resolution was set at 1200 dpi to ensure sufficient visualization of midrib and major veins. For both methods, image sequences were then analysed manually according to Brodrribb *et al.* (2016, 2017) using Fiji (Schindelin *et al.*, 2012). Briefly, embolism formation can be identified and quantified by subtracting consecutive images as changes in the grey level associated with vascular tissue. The ‘Analyse Particles’ function was used to measure the area of embolized pixels in each image, and threshold analyses were used to remove noise related to leaf movement from drying. The percentage of embolized area for each image was calculated as the amount of embolism cumulated and the total embolized area of the scanned area incorporating only major vein orders.

The vulnerability curves to cavitation were obtained by plotting the leaf water potential (Ψ_{Leaf}) measured regularly, that is once or twice a day depending on the dehydration rate of the tree, in three different neighbour leaves using a Scholander-type pressure chamber (PMS), against the percentage of embolized pixels (PEP: % of total). P_{50} (the Ψ_{Leaf} value at which 50% of the xylem cavitation events had been observed) was determined by fitting a sigmoid using Eqn 1 (Pammenter & Vander Willigen, 1998) where a is the slope of the curve at the inflexion point:

$$\text{PEP} = \frac{100}{1 + e^{a(\Psi_{\text{Leaf}} - P_{50})}} \quad \text{Eqn 1}$$

Ψ_{Leaf} values inducing 50%, 12% and 88% of xylem cavitation (i.e. P_{50} , P_{12} and P_{88} respectively) were computed using the R FITPLC package (Duursma & Choat, 2017).

Water status, leaf relative water content and electrolyte leakage

Over the progressive bench dehydration of each individual used for constructing the leaf vulnerability curves, regular samplings of three to five leaves (depending on leaf material availability) were carried out for assessing the water status and cellular integrity of each individual. Briefly, Ψ_{Leaf} , leaf relative water content (RWC_{Leaf}) and leaf cellular integrity through the percentage of EL were measured on those leaves.

Ψ_{Leaf} was measured using a Scholander-type pressure chamber (PMS), while RWC_{Leaf} was measured and calculated according to Barrs & Weatherley (1962). Briefly, for RWC_{Leaf} , leaves were cut and immediately placed in a vial to prevent further desiccation. RWC_{Leaf} was then calculated according to Eqn 2:

$$\text{RWC} = \frac{(\text{FW} - \text{DW})}{(\text{TW} - \text{DW})}, \quad \text{Eqn 2}$$

where FW is the fresh weight measured immediately after sampling, TW is the turgid weight measured after immersing the leaf in distilled water for 24 h and DW is the dry weight of samples after 24 h of drying in an oven at 70°C. All measurements were done using a precision scale (Mettler ME 204; Mettler Toledo).

For *E. viminalis* and *L. nobilis*, and at RWC values lower than 30% and 25% respectively, a decrease in the ratio (Eqn 3) was observed (Fig. S1) indicating an incapacity of the sample to rehydrate to full turgor that would provoke an overestimation of the RWC (John *et al.*, 2018; Abate *et al.*, 2021).

$$\frac{\text{TW} - \text{DW}}{\text{DW}} \quad \text{Eqn 3}$$

Thus, as the ratio (Eqn 3) of rehydrated samples is supposed to be constant if the cells do not lose their rehydration ability, the TW of the samples showing a decreased ratio (Eqn 3) was recomputed using the average ratio (Eqn 3) determined for each species on the samples collected above the determined threshold value for full rehydration (i.e. on samples showing a $\text{RWC} > 30\%$ for *E. viminalis* and $> 25\%$ for *L. nobilis*). Then, the RWC was recalculated according to Eqn 2 replacing the TW value by the recomputed TW.

Electrolyte leakage was measured using an adapted protocol of the original EL protocol of Zhang & Willison (1987) and Sutinen *et al.* (1992). Each leaf was cut in 1 mm slices using a pair of scissors and immersed in test tubes containing 15 ml of pure water. Test tubes were shaken at 60 shakes min^{-1} overnight at 5°C to stop enzyme activity. Water conductivity of the effusate (C1) was then measured at room temperature (c. 22°C) using a conductimeter (SevenCompact S230; Mettler Toledo) and a sensor with a measuring range of 0.001–500 $\mu\text{S cm}^{-1}$ (Cell Cond InLab 741; Mettler Toledo). After C1 measurement, all living cells were killed by autoclaving the samples at 121°C for 30 min (King & Ludford, 1983). Measurement of the effusate maximal conductivity (C2) was then done at room temperature. The EL was then determined as:

$$\text{EL} = \frac{C1}{C2} \times 100 \quad \text{Eqn 4}$$

Electrolyte leakage values were normalized between 0 and 100 to define a minimum and maximum level of cellular damage by using the mean value of the 10 lowest points and the 10 maximum points.

Cavitation and cellular death dynamics regarding cellular water stress: nonlinear regressions and sigmoid parameters

The images obtained with the optical method for determining the leaf vulnerability curve to cavitation were reused to determine the level of embolism over the decrease in RWC_{Leaf} . Using the RWC_{Leaf} data collected as described previously and a linear regression in phases, we calculated the RWC_{Leaf} for each individual and associated each image with a RWC_{Leaf} value. We then plotted the RWC_{Leaf} against PEP for six to eight individuals per species. The RWC_{50} (the RWC_{Leaf} value at which 50% of the xylem cavitation events had been observed) was determined by fitting a sigmoid using Eqn 5 (Pammenter & Vander Willigen, 1998), where a is the slope of the curve at the inflexion point:

$$PEP = \frac{100}{(1 + e^{a(RWC_{Leaf} - RWC_{50})})} \quad \text{Eqn 5}$$

By analogy with the P_{12} and P_{88} points, RWC_{12} and RWC_{88} representing the RWC_{Leaf} value associated with 12% and 88% loss of hydraulic conductance were computed using the FITPLC R package (Duursma & Choat, 2017) replacing the Ψ_{Leaf} inputs with the RWC_{Leaf} values (Fig. 1).

In order to visualize the dynamic of cell damage as the RWC_{Leaf} decreased, the percentage of EL was plotted against RWC_{Leaf} for each species. A nonlinear regression (NLS), four-parameter logistic regression, was fitted using SIGMAPLOT with Eqn 6:

$$NLS = \min + \frac{(\max - \min)}{1 + \frac{x}{EL_{50}} - Hillslope} \quad \text{Eqn 6}$$

where EL_{50} represents the RWC_{Leaf} value at which 50% of the cells are dead, max and min represent the maximum and

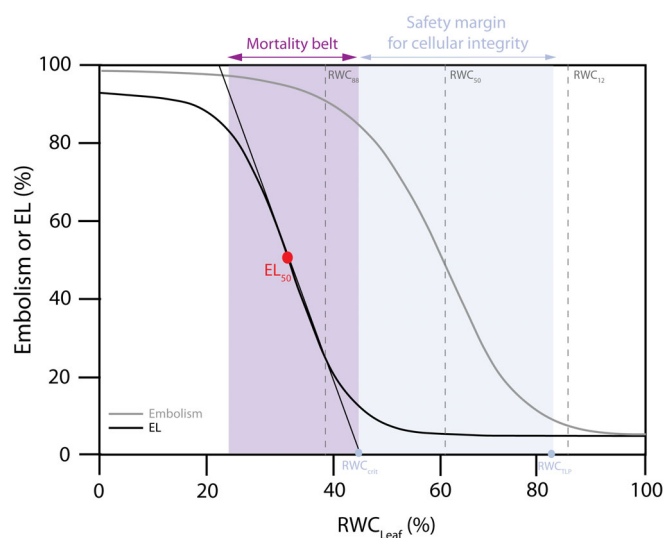


Fig. 1 Conceptual figure representing, in blue, the safety margin to cellular integrity in between the leaf relative water content at turgor loss (RWC_{TLP}) and the critical leaf RWC (RWC_{crit}) and in purple the mortality belt defined through the slope of the tangent of the electrolyte leakage (EL) regression at the midpoint (EL_{50}). Dashed grey lines represent the RWC values at which 12% (RWC_{12}), 50% (RWC_{50}) and 88% (RWC_{88}) of the vessels are embolized.

minimum EL value of the dataset, and Hillslope represents the slope of the regression at the inflexion point.

From this NLS fitting was extracted the critical level of RWC (RWC_{crit}) below which the cells start to incur damage from water stress. By analogy with the air entry pressure defined by Meinzer *et al.* (2009) and Torres-Ruiz *et al.* (2017), the RWC_{crit} was determined at the x -intercept of the tangent through the midpoint (EL_{50}) of the NLS regression curve and corresponded to 12% of cell damage (Fig. 1). The slope of the regression was used to determine the ‘Mortality Belt’ (Fig. 1), that is the range in which the decrease in RWC_{Leaf} provokes the maximum cell damage. Combining the EL NLS fitting and the leaf material properties, we calculated, for each species, a safety margin for cellular integrity in between RWC_{TLP} and RWC_{crit} (Fig. 1). RWC_{TLP} was used as the starting point of the safety margin for cellular integrity, serving as a proxy for stomatal closure and corresponding therefore to an important reduction in water losses that prevents an important decrease in RWC.

X-ray micro-CT anatomical analyses

Synchrotron-based X-ray micro-CT was used to visualize the shape of the cells within the leaf blade of the three studied species at different RWC. Fifteen leaves sampled from 10 *E. viminalis* individuals, 16 leaves from eight *L. nobilis* individuals and 10 leaves from six *P. tremula* × *alba* individuals were scanned between 8 September and 14 September 2020, at the French synchrotron facility SOLEIL (Paris, France) using the micro-CT PSICHE beamline. Two weeks before the scans, irrigation was withheld progressively in the different trees in order to generate a wide range of Ψ_{Leaf} and RWC_{Leaf} at the time of scanning.

The leaf of interest was scanned using a high-flux ($3.1011 \text{ photons mm}^{-2}$) 25-keV monochromatic X-ray beam. The projections were recorded with a Hamamatsu Orca Flash sCMOS Camera (Hamamatsu Photonics KK, Shizuoka, Japan) equipped with a 250- μm -thick LuAG Scintillator and visible light optics providing an effective pixel size of $0.3 \mu\text{m}$. The complete tomographic scan included 2048 projections, 50 ms each, for a 180° rotation. Samples were exposed for 75 s to the X-ray beam. Tomographic reconstructions were performed using PyHST2 software (Mirone *et al.*, 2014) employing the method of Paganin (2006). Each leaf scan led to a volume of 2048 images. For each species, three images were extracted from the volumes of five (*E. viminalis*, *L. nobilis*) or six (*P. tremula* × *alba*) samples and were analysed using Fiji software (Schindelin *et al.*, 2012). The different leaf tissues, that is epidermis, palisade parenchyma and spongy parenchyma, were outlined in three to five slices per stack using the freehand selection tools, and their area determined in μm^2 using the measuring tool of Fiji (Schindelin *et al.*, 2012).

At the same time of the scan, three leaves located next to the scanned leaf were used to measure Ψ_{Leaf} with a Scholander-type pressure chamber (Precis 2000, Gradignan, France). Three other nearby leaves were used to determine the RWC_{Leaf} and three others were used to determine the EL.

Measurements of leaf light transmittance

During the experiments allowing to generate the vulnerability curves to cavitation, obvious colour changes occurred. In the 8-bit image stacks, these changes could be detected as a darkening of the leaf tissue, and thus the stack of images was used to monitor changes in greyscale (Brodribb *et al.*, 2021). For this, using Fiji software (Schindelin *et al.*, 2012) and the command ‘measure stack’ from the OSOV Toolbox, we measured the grey mean value for each image of the stack. The loss in light transmittance was then calculated as the percentage of maximum.

A second noticeable change in leaf colour (i.e. blackening), more intense than the darkening observed along the dehydration, was noticed after full embolization of the vessels at very low RWC_{Leaf} and started at the edges of the leaf. Therefore, measurements of the leaf light transmittance were made in the visibly different regions of the leaf. Considering this, synchrotron-based X-ray micro-CT scans were performed on the different regions of the leaf, that is in a section with a high light transmittance and in a section with a low light transmittance, allowing distinction of anatomical changes.

Results

Turgor loss point and leaf resistance to cavitation

Pressure–volume curves (Fig. S2) allowed determining both TLP and ϵ for each species. Ψ_{TLP} occurred at -1.38 MPa for *P. tremula* \times *alba*, -1.61 MPa for *E. viminalis* and -2.46 MPa for *L. nobilis* corresponding to RWC_{TLP} values of 88.24%, 88.05%

and 90.65% respectively (Table 1). ϵ was 10.88, 10.22 and 15.56 MPa for *P. tremula* \times *alba*, *E. viminalis* and *L. nobilis* respectively (Table 1). Xylem vulnerability curves (Fig. S3) resulted in P_{50} values of -1.96 , -3.23 and -5.17 MPa for *P. tremula* \times *alba*, *E. viminalis* and *L. nobilis* respectively (Table 1).

Dying of thirst?

On the observed sigmoidal opposed dynamics for RWC_{Leaf} and the percentage of embolism during dehydration (Fig. 2), three different phases could be distinguished for each species. A first phase between the maximal RWC_{Leaf} at Ψ_{Leaf} values of *c.* 0 MPa and Ψ_{TLP} where RWC_{Leaf} diminished slowly and the amount of embolism remains close to zero; a second phase after reaching the Ψ_{TLP} concomitant to a significant increase in embolism until P_{88} where the RWC_{Leaf} decreased exponentially; and a third phase after HF (P_{88}) where only residual losses of water occurred and RWC_{Leaf} decreased slightly until reaching a steady state. During the first phase, a decrease in RWC_{Leaf} of *c.* 16% for *P. tremula* \times *alba*, *c.* 5% for *E. viminalis* and *c.* 13% *L. nobilis* was observed. Therefore, at Ψ_{TLP} , embolism levels of 20.0%, 3.3% and 8.2% were observed for *P. tremula* \times *alba*, *E. viminalis* and *L. nobilis* respectively. During the second phase, as the level of embolism reached 88%, RWC_{Leaf} decreased from 75.8% to 45.6% for *P. tremula* \times *alba*, from 83.4% to 51.7% for *E. viminalis* and from 76.3% to 27.4% for *L. nobilis*. During the third phase, that is after reaching P_{88} , RWC_{Leaf} continued to decrease until reaching a RWC_{Leaf} steady state of *c.* 20% for *P. tremula* \times *alba* and *L. nobilis* and *c.* 37% for *E. viminalis*.

Table 1 Parameters extracted for each species.

Parameter	<i>Populus tremula</i> \times <i>alba</i>	<i>Eucalyptus viminalis</i>	<i>Laurus nobilis</i>
Ψ_{TLP} (MPa)	$-1.38 (\pm 0.2 \text{ SE})$	$-1.61 (\pm 0.23 \text{ SE})$	$-2.46 (\pm 0.45 \text{ SE})$
RWC_{TLP} (%)	88.24 ($\pm 1.80 \text{ SE}$)	88.05 ($\pm 3.85 \text{ SE}$)	90.65 ($\pm 2.09 \text{ SE}$)
ϵ (MPa)	10.88 ($\pm 1.21 \text{ SE}$)	10.22 ($\pm 2.24 \text{ SE}$)	15.56 ($\pm 5.40 \text{ SE}$)
P_{12} (MPa)	$-1.05 \text{ CI } [-1.09; -1.01]$	$-2.28 \text{ CI } [-2.34; -2.23]$	$-2.95 \text{ CI } [-3.02; -2.88]$
P_{50} (MPa)	$-1.96 \text{ CI } [-1.99; -1.94]$	$-3.23 \text{ CI } [-3.26; -3.20]$	$-5.17 \text{ CI } [-5.22; -5.13]$
P_{88} (MPa)	$-2.88 \text{ CI } [-2.92; -2.84]$	$-4.17 \text{ CI } [-4.20; -4.15]$	$-7.39 \text{ CI } [-7.46; -7.32]$
RWC_{12} (%)	80.95 CI [80.03; 81.88]	77.74 CI [75.72; 79.88]	63.01 CI [62.70; 63.31]
RWC_{50} (%)	61.66 CI [61.13; 62.14]	60.99 CI [60.12; 61.98]	51.40 CI [51.18; 51.65]
RWC_{88} (%)	42.38 CI [41.33; 43.28]	44.23 CI [43.41; 44.98]	39.80 CI [39.53; 40.08]
Ψ_{crit} (MPa)	$-0.70 \text{ CI } [-1.18; -0.23]$	$-2.81 \text{ CI } [-2.96; -2.68]$	$-3.27 \text{ CI } [-3.42; -2.99]$
RWC_{crit} (%)	69.04 CI [65.90; 73.43]	56.36 CI [55.23; 58.10]	54.95 CI [52.60; 59.50]
Safety margin (%RWC)	20.00	31.69	35.70
EL_{50} (MPa)	$-2.98 (\pm 0.28 \text{ SE})$	$-6.15 (\pm 0.31 \text{ SE})$	$-5.95 (\pm 0.23 \text{ SE})$
EL_{50} (%RWC)	42.56 ($\pm 1.45 \text{ SE}$)	41.75 ($\pm 0.69 \text{ SE}$)	36.17 ($\pm 1.09 \text{ SE}$)
EL_{max} (%RWC)	16.09 CI [13.24; 17.76]	27.13 CI [25.46; 28.12]	17.39 CI [15.43; 17.56]
Slope NLS	$-3.21 (\pm 0.34 \text{ SE})$	$-5.71 (\pm 0.52 \text{ SE})$	$-3.85 (\pm 0.51 \text{ SE})$

Ψ_{TLP} and RWC_{TLP} represent, respectively, the water potential and relative water content (RWC) value at the turgor loss point. ϵ represents the cell modulus of elasticity. P_{12} , P_{50} and P_{88} correspond to the water potential value inducing 12%, 50% and 88% of loss of xylem hydraulic conductance respectively. RWC_{12} , RWC_{50} and RWC_{88} represent the RWC value encountered at 12%, 50% and 88% of loss of xylem hydraulic conductance respectively. Ψ_{crit} and RWC_{crit} symbolize the water potential and RWC values at which cell integrity begins to be compromised by dehydration. The safety margin designates the decrease between the leaf RWC_{TLP} and RWC_{crit} . EL_{50} represents the water potential value or RWC value at which 50% of cell damage is encountered. EL_{max} designates the RWC value at which 100% of cell damage is encountered. Slope nonlinear regression corresponds to the slope of the regression and represents the rate of cellular mortality. The confidence intervals are provided in brackets, while the standard errors are indicated in parenthesis.

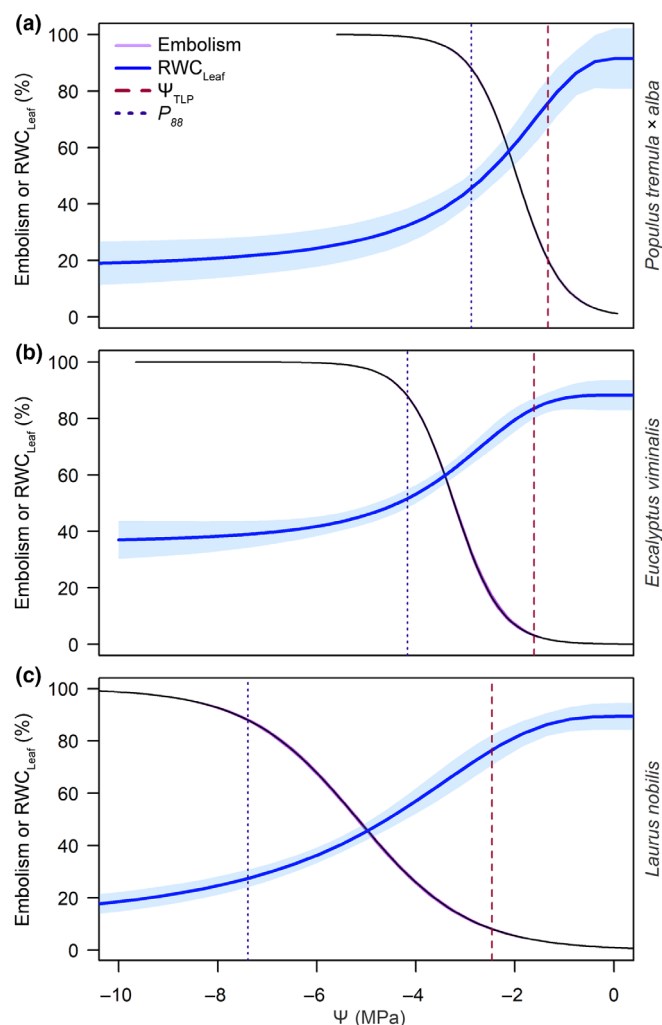


Fig. 2 Dynamic of embolism propagation and leaf relative water content (RWC_{Leaf}) regarding a decrease in water potential (Ψ) for (a) *Populus tremula* \times *alba*, (b) *Eucalyptus viminalis* and (c) *Laurus nobilis*. Red dashed lines represent turgor loss point. Purple dashed lines represent 88% of loss of hydraulic conductance. 95% confidence intervals are represented by shading.

Dynamic of cavitation and cell mortality

When combining together leaf physiological traits, embolism and EL vs RWC_{Leaf} (Fig. 3), our results clearly showed that cavitation events occurred at higher RWC_{Leaf} values than the onset of cell damage. Indeed, RWC_{12} was constantly higher than RWC_{crit} (Table 1; Fig. 3). The decreases in RWC_{Leaf} between the onset of cavitation and the onset of cell damage were estimated as 11.84% for *P. tremula* \times *alba*, 21.38% for *E. viminalis* and 8.06% for *L. nobilis*.

For the three species, higher embolism levels than EL (Fig. 3) were found at any RWC_{Leaf} value. Consequently, for a level of embolism equal to 50%, the levels of EL were of 23.38% for *P. tremula* \times *alba*, 5.97% for *E. viminalis* and 22.26% for *L. nobilis*. Also, at a percentage of embolism equal to 88%, *P. tremula* \times *alba* showed an EL level of 50.42%, *E. viminalis* an EL level of 36.80% and *L. nobilis* an EL level of 47.56%. EL_{50} was

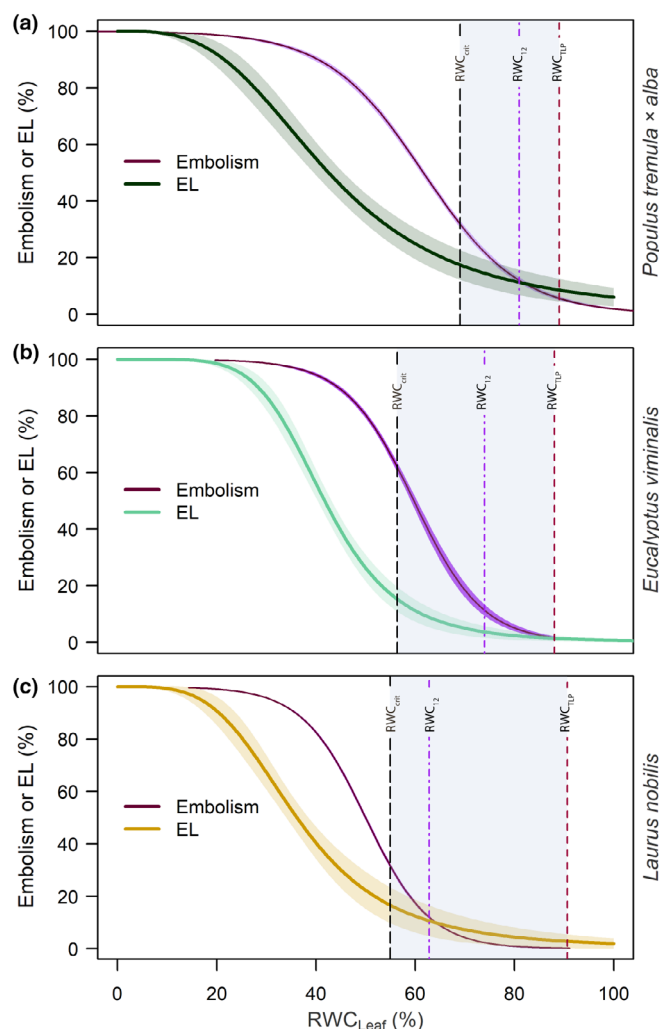


Fig. 3 Dynamic of embolism propagation and cellular damage (EL) regarding a decrease in leaf relative water content (RWC_{Leaf}) for (a) *Populus tremula* \times *alba*, (b) *Eucalyptus viminalis* and (c) *Laurus nobilis*. Blue shaded areas represent the safety margin for cellular integrity calculated between the leaf relative water content at the point of turgor loss (RWC_{TLP} , red dashed line) and the critical leaf RWC (RWC_{crit} , black dashed line). Violet dashed lines represent the RWC value at which 12% of xylem embolism is observed. 95% confidence intervals are represented by shading.

observed at embolism degrees of 88%, 92.97% and 89.63% for *P. tremula* \times *alba*, *E. viminalis* and *L. nobilis* respectively. The maximum level of cell damage (EL_{max}) was always subsequent to a 100% amount of embolism for all species.

A more drought-resistant xylem, more resistant cells?

Populus tremula \times *alba* which had reported the lowest resistance to cavitation ($P_{50} = -1.96$ MPa) also presented the highest RWC_{crit} (69.04%) making its cells the least resistant to dehydration (Fig. 4; Table 1). *Laurus nobilis* showed the highest resistance to cavitation ($P_{50} = -5.17$ MPa), and at the same time, the lowest RWC_{crit} (54.95%) showed no differences with *E. viminalis*, which has a P_{50} of -3.24 MPa and presented a RWC_{crit} of 56.36% (Fig. 4; Table 1).

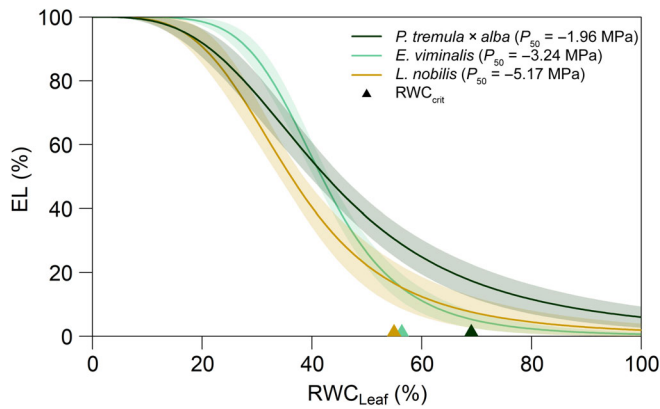


Fig. 4 Dynamic of cellular damage (EL) regarding leaf relative water content (RWC_{Leaf}). Triangles represent the critical leaf RWC (RWC_{crit}) identified for each species. 95% confidence intervals are represented by shading.

When calculating a safety margin for cell integrity in between RWC_{TLP} and RWC_{crit} , the species' resistance to cavitation and their safety margin to cellular damage were not correlated. Indeed, *E. viminalis* and *L. nobilis* presented similar safety margins, whereas *P. tremula* × *alba* presented a much narrower one (Fig. 3; Table 1).

EL_{50} corresponded to an RWC_{Leaf} value of 42.56%, 41.75% and 36.17% for *P. tremula* × *alba*, *E. viminalis* and *L. nobilis* respectively (Table 1). EL_{50} was thus found at lower RWC_{Leaf} values in *L. nobilis* leaves that presented a higher xylem resistance to cavitation, that is lower P_{50} . EL_{50} showed no differences between *P. tremula* × *alba* and *E. viminalis* despite the difference in P_{50} .

When comparing the slope of the NLS regressions, *E. viminalis* presented a narrower mortality belt than *P. tremula* × *alba* and *L. nobilis*, which showed a similar mortality belt (Table 1).

The process of cell death: X-ray insights

X-ray micro-CT imaging revealed anatomical changes as RWC_{Leaf} decreased and EL increased, with the more evident changes occurring at the mesophyll level (Fig. 5). Through the course of dehydration, the mesophyll area was reduced by a factor of 2.95 for *P. tremula* × *alba*, whereas the reduction in epidermis area was only 1.70. The same pattern was observed for both *E. viminalis* and *L. nobilis*, which presented a mesophyll area reduction of 2.09 and 1.81 respectively. However, while *E. viminalis* showed a reduction in its epidermis area of 1.47, no changes were observed for *L. nobilis*.

The first mesophyll structural changes under decreasing RWC_{Leaf} occurred at the palisade layer for both *P. tremula* × *alba* and *L. nobilis* (Figs 5, 6). However, a different pattern was observed for *E. viminalis* with, first, a conjoint dehydration of the spongy and palisade parenchyma (Figs 5, 6). In a second time, as the RWC_{Leaf} continued decreasing, main anatomical changes were observed in the spongy parenchyma, which showed an important reduction in cell area for the three species (Figs 5, 6). Ultimately, and only in the case of *L. nobilis*, a secondary conjoint reduction in the palisade and spongy areas happened.

Leaves of all three species visually became darker as the RWC_{Leaf} decreased. Concomitant to the decrease in RWC_{Leaf} and after a significant reduction in cell area occurred at the different cell layers, leaf light transmittance dropped. The start of the loss in leaf light transmittance was synchronized with the start of the increase in EL for all three species. For *P. tremula* × *alba* and *L. nobilis*, the loss in light transmittance was synchronized with the full dynamic of EL. However, for *E. viminalis*, the maximum loss in light transmittance was attained before reaching the maximum level of EL (Fig. 5).

After full embolization of the leaf veins, an abrupt blackening easily detectable by the naked eye occurred within the leaf (Figs 7a, S4). Synchrotron-based X-ray micro-CT scans were performed within a single leaf at different locations presenting differences in light transmittance values (Figs 7a,b, S4) and showed that epidermis cells became air-filled (Figs 7c, S4).

Discussion

Our results evince that, during the progressive dehydration of trees, xylem cavitation precedes cellular death at the leaf level. Indeed, the onset of cell dehydration-induced damage happens at lower RWC_{Leaf} values than the ones at which the onset of xylem cavitation occurred. In addition, RWC_{crit} , the critical water status level inducing cell damage, occurred at varying embolism levels depending on the species (c. 30% for *P. tremula* × *alba* and *L. nobilis*, and c. 61% for *E. viminalis*). Considering this, our results show that by compromising water delivery to the leaf mesophyll, cavitation provokes a decrease in RWC_{Leaf} that is followed by an increase in cellular damage in woody species. These results agree with a recent study on tomato mutants showing that leaf vein cavitation immediately compromised local water supply to the leaf mesophyll enrolling the tissues to death (Brodrribb *et al.*, 2021). However, when evaluating such compromise at the whole leaf level, our results suggest that low levels of embolized vessels have no immediate effect on the amount of living cells probably due to higher tolerance to hydraulic disruption provided by the vascular redundancy of the leaves (Sack *et al.*, 2008). Indeed, despite the important variation in cell volume observed at the onset of dehydration when trees still show relatively high values of RWC_{Leaf} , no events of cell mortality were encountered.

Different species and different cell death dynamic

During dehydration, leaves first showed a significant loss in turgor pressure followed by a progressive cavitation of the leaf veins preceding the appearance of the first cellular structural damage. The RWC_{Leaf} values at which these three processes occur and the differences between them could vary across species according to their resistance to drought. This sequence of events is consistent with the findings of Creek *et al.* (2020) where stomatal closure, which typically occurs at water potential values similar to those for TLP (Brodrribb *et al.*, 2003; Bartlett *et al.*, 2016; Trueba *et al.*, 2019), preceded xylem cavitation, and with those of Guadagno *et al.* (2017) where cellular damage occurred after turgor loss. In our study, RWC_{crit} varied across species but showed no

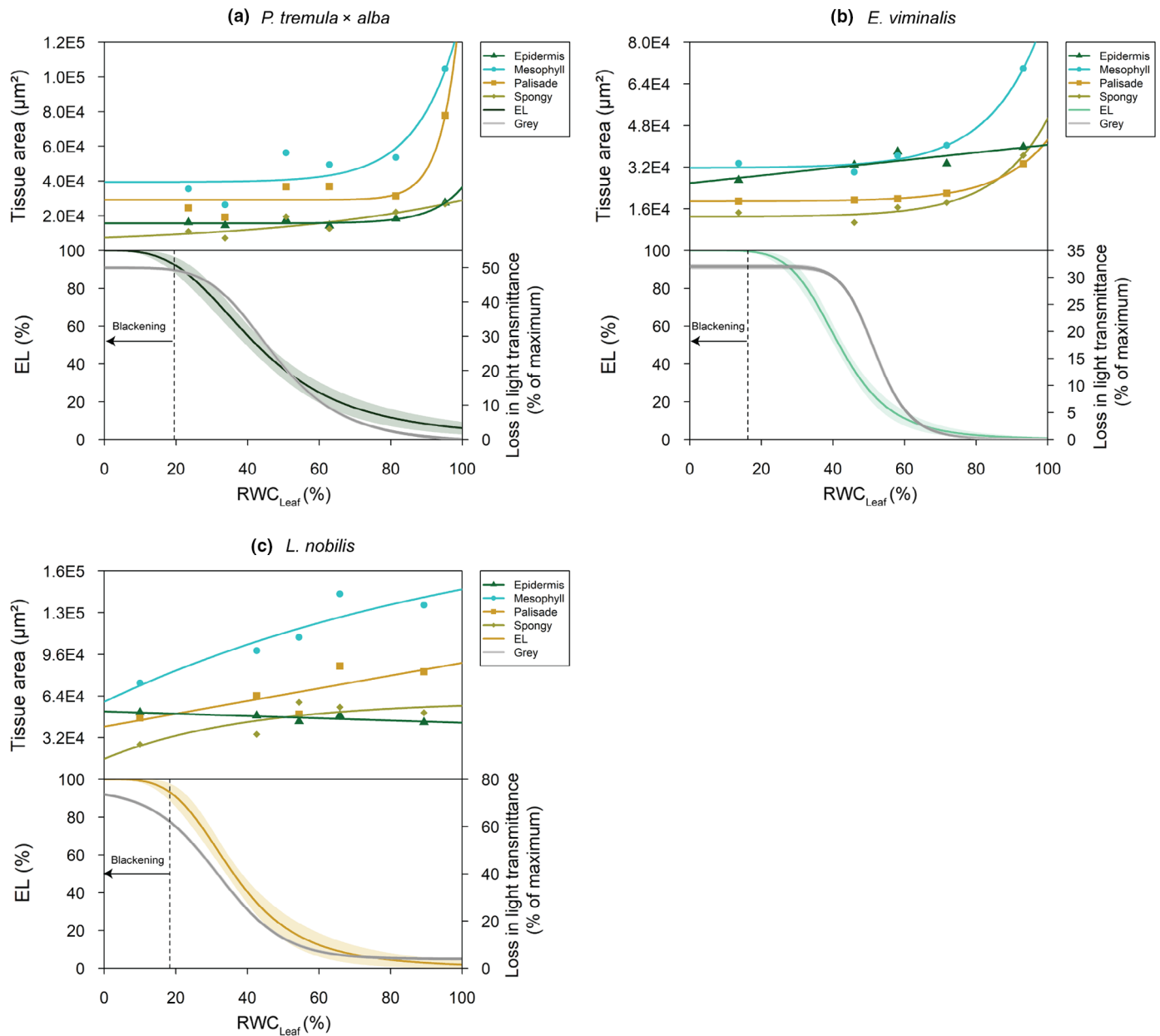


Fig. 5 Evolution of the area (in μm^2) of leaf epidermis, palisade parenchyma, spongy parenchyma and overall mesophyll as well as cellular damage (EL) and loss in leaf light transmittance regarding a decrease in leaf RWC (RWC_{Leaf}) for (a) *Populus tremula* × *alba*, (b) *Eucalyptus viminalis* and (c) *Laurus nobilis*. Black dashed lines symbolize the RWC_{Leaf} at which a visual blackening of the samples was observed. 95% confidence intervals are represented by shading. Area measurements were done using synchrotron-based X-ray micro-CT images obtained on dehydrating leaves and analysed with Fiji software.

linear relationship with P_{50} . Indeed, despite a noticeable difference in P_{50} , *E. viminalis* and *L. nobilis* presented similar RWC_{crit} values (c. 55%). On the contrary, the least resistant to cavitation species, *P. tremula* × *alba*, presented a RWC_{crit} higher than the one of the two other species. These findings highlight that, although RWC_{TLP} is relatively constant between species (Bartlett *et al.*, 2012), RWC_{crit} for cell damage might be species-dependent. This species dependency could be linked to the structure and composition of the cells themselves and their capacity to respond to changes in turgor by either relaxing or tightening the cell wall (Moore *et al.*, 2008), thus preventing cell deformation and shrinkage to lethal level (Scoffoni *et al.*, 2014), and death

from cytorrhysis, that is when the cell shrinks as a unit (Oertli, 1986; Taiz & Zeiger, 2006).

Our results evinced that, while showing different resistance to cavitation and different RWC_{crit} , the slope of the NLS regression determining the mortality belt was not linearly correlated with P_{50} as similar slopes were encountered for two of the three species studied, that is *P. tremula* × *alba* and *L. nobilis*. Thus, it could be expected for those two species that the same cell mortality rate would be observed after reaching their respective RWC_{crit} if the RWC_{Leaf} keeps declining at the same pace for the two species. Therefore, this highlights the importance of considering the dehydration rate of the organs and the pace of dehydration during

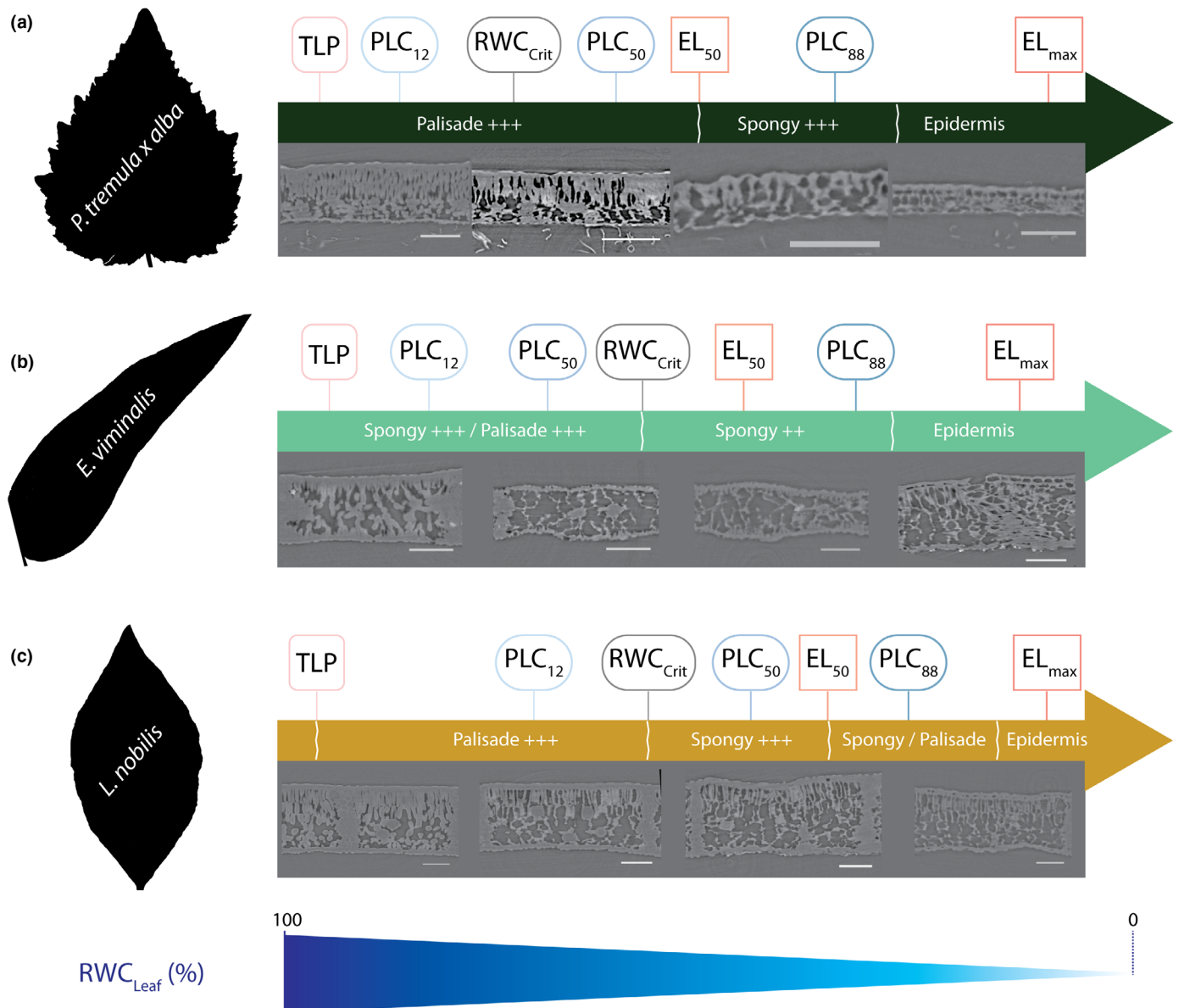


Fig. 6 Sequence of events and corresponding synchrotron-based X-ray micro-CT images, leading to maximal cellular death (EL_{max}) regarding a decrease in leaf RWC (RWC_{Leaf}) for (a) *Populus tremula* × *alba*, (b) *Eucalyptus viminalis* and (c) *Laurus nobilis*. Bar, 100 μ m. TLP stands for turgor loss point; PLC_{12} , PLC_{50} and PLC_{88} represent the RWC_{Leaf} at which 12%, 50% and 88% of loss of xylem conductance are encountered respectively; RWC_{crit} represents the critical leaf RWC identified for each species; EL_{50} symbolizes the RWC value at which 50% of cellular damage is encountered.

drought and after stomatal closure, for example residual transpiration (Billon *et al.*, 2020) when aiming to determine the timing of cell death, and consequently, tissue and organ death, after turgor loss.

A closer look at the sequence of cell damage

Changes in leaf light transmittance and leaf colour have been attributed to the collapse of palisade cells, therefore serving as a proxy for determining leaf cell mortality (Brodrribb *et al.*, 2021). By providing a quantification of cellular death through EL measurements, our results confirm the hypothesis of a correlation

between a decrease in RWC_{Leaf} , leaf light transmittance and cellular death made by Brodrribb *et al.* (2021). However, by performing measurements in different cells layers within the leaf, our study provides a more detailed analysis of the location of the structural changes occurring in leaves during dehydration (Fig. 6). Our results suggest a decrease in mesophyll cell volume, which agrees with the results of Momayyezi *et al.* (2022) where *Juglans regia* L. and *Juglans microcarpa* leaves also exhibited drought-induced reductions in mesophyll cell volume, which should be correlated with cellular death (Mantova *et al.*, 2022). Indeed, cell death via membrane damage could occur through physical constraints (Mantova *et al.*, 2022) such as cell cavitation,

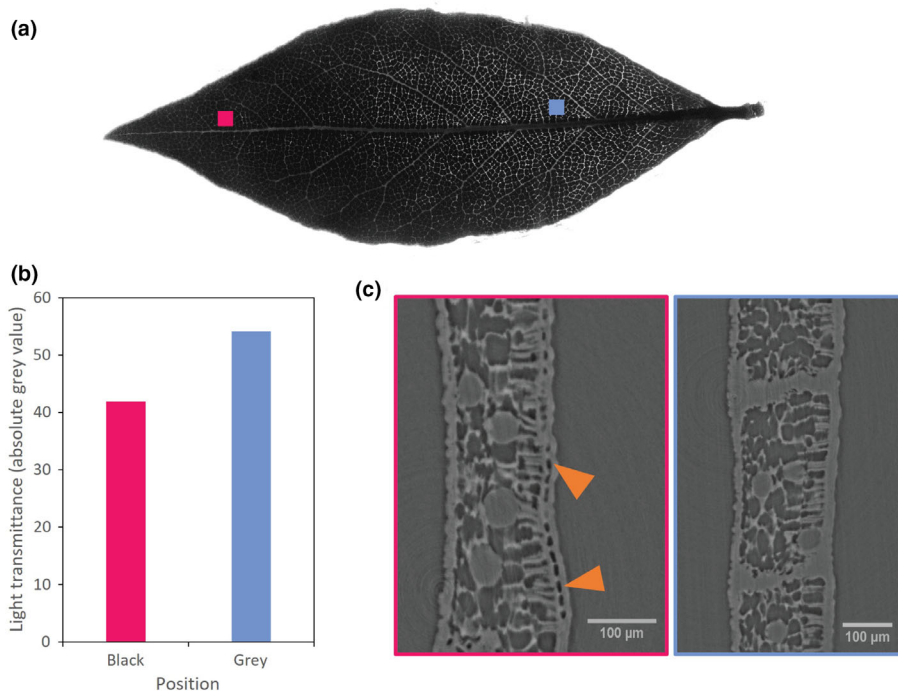


Fig. 7 Damage at the epidermis level after full embolization of the xylem vessels for *Laurus nobilis*. (a) Scan of a *L. nobilis* leaf ($RWC_{\text{Leaf}} = 18.19\%$, $EL = 90.93\%$) obtained in transmitted light. Leaf light transmittance differs within the leaf at the positions marked in red and blue. (b) Measurements of light transmittance in absolute grey value performed with Fiji software at the respective red and blue positions. (c) Synchrotron-based X-ray micro-CT images obtained on the same *L. nobilis* leaf. The position of each scan is indicated by either the blue or red rectangles on the transmitted light image (a). Orange triangles point at the epidermis cells and indicate the structural changes observed.

that is when a critical pressure in the cell is reached causing the cytoplasm fractures and the formation of a gas bubble (Sakes *et al.*, 2016) and/or cytorrhysis (Oertli, 1986; Taiz & Zeiger, 2006). However, the cell shrinkage observed in our experiment was not always associated with cellular death. In fact, depending on the species, the mesophyll cells could endure a differential reduction in cell volume before showing an increment in EL. Indeed, the mesophyll cells of *P. tremula* and *E. viminalis* were able to support an important volume reduction at the beginning of the dehydration that was not associated with cell mortality. However, for *L. nobilis*, such reduction in mesophyll cell volume was immediately correlated with an increase in cell mortality. Looking closely at the sequence of events, the palisade, spongy and epidermis cells responded differently to dehydration. In the case of *P. tremula* × *alba* and *L. nobilis*, the palisade cells were the first affected by dehydration, whereas there were no differences in the timing of cell volume reduction for the spongy and palisade cells of *E. viminalis*. Ultimately and for all three species, the epidermis cells were the last affected by drought. These differences in response to cell changes in volume could be linked to the size, structure and composition of the cells *per se* as those components might influence the rigidity of the cell wall and thus favour or prevent shrinkage to lethal level (Scoffoni *et al.*, 2014; Joardder *et al.*, 2015).

Our results also highlight that a visual blackening of the leaf occurring at very low RWC, and once the leaf was fully embolized, was provoked by changes happening in the epidermis cells only after strong structural changes were observed in the mesophyll and once most of the leaf living tissues were dead according to the high levels of EL. Epidermis cells were the last prone to structural changes for the three species and somehow became air-filled when reaching very low RWC_{Leaf} values, provoking a

blackening of the leaf that is distinguishable to the naked eye. However, even though our scans reached a precision of $0.3 \mu\text{m}$, micro-CT observations were not precise enough to determine which of the two mechanisms (i.e. cell cavitation or cytorrhysis) induced air-filling in epidermis cells at such low RWC_{Leaf} values. Other microscopy imaging techniques would be required to further investigate the specific mechanisms inducing mortality at the cellular level under drought conditions.

Die or survive?

In general, leaves showed 50% of cell death once they reached an amount of embolism relatively high (i.e. $> 80\%$) for the three species studied. The highest levels of cellular death were observed only after the leaves were almost fully embolized. Therefore, considering the results of Mantova *et al.* (2021) and Vilagrosa *et al.* (2010) showing how the capacity of recovery after drought could be related to the amount of living cells remaining at the time of rewating, our results raise new questions on the extent to which cell mortality would lead to organ death. We hypothesize that, with an estimated 45.91% of living cells at levels of embolism of *c.* 90%, it is less likely for *P. tremula* × *alba* leaves to recover from drought than for *E. viminalis*, the leaves of which showed 55.47% of living cells at a similar embolism level. Determining the critical percentage of cell mortality for organ survival is crucial to precisely elucidate the capacity of an organ and therefore of the tree to recover after being exposed to drought (Fig. 8).

Conclusion and perspectives

By evaluating the variation in RWC_{Leaf} , EL and the level of embolism in leaves from trees exposed to a progressive

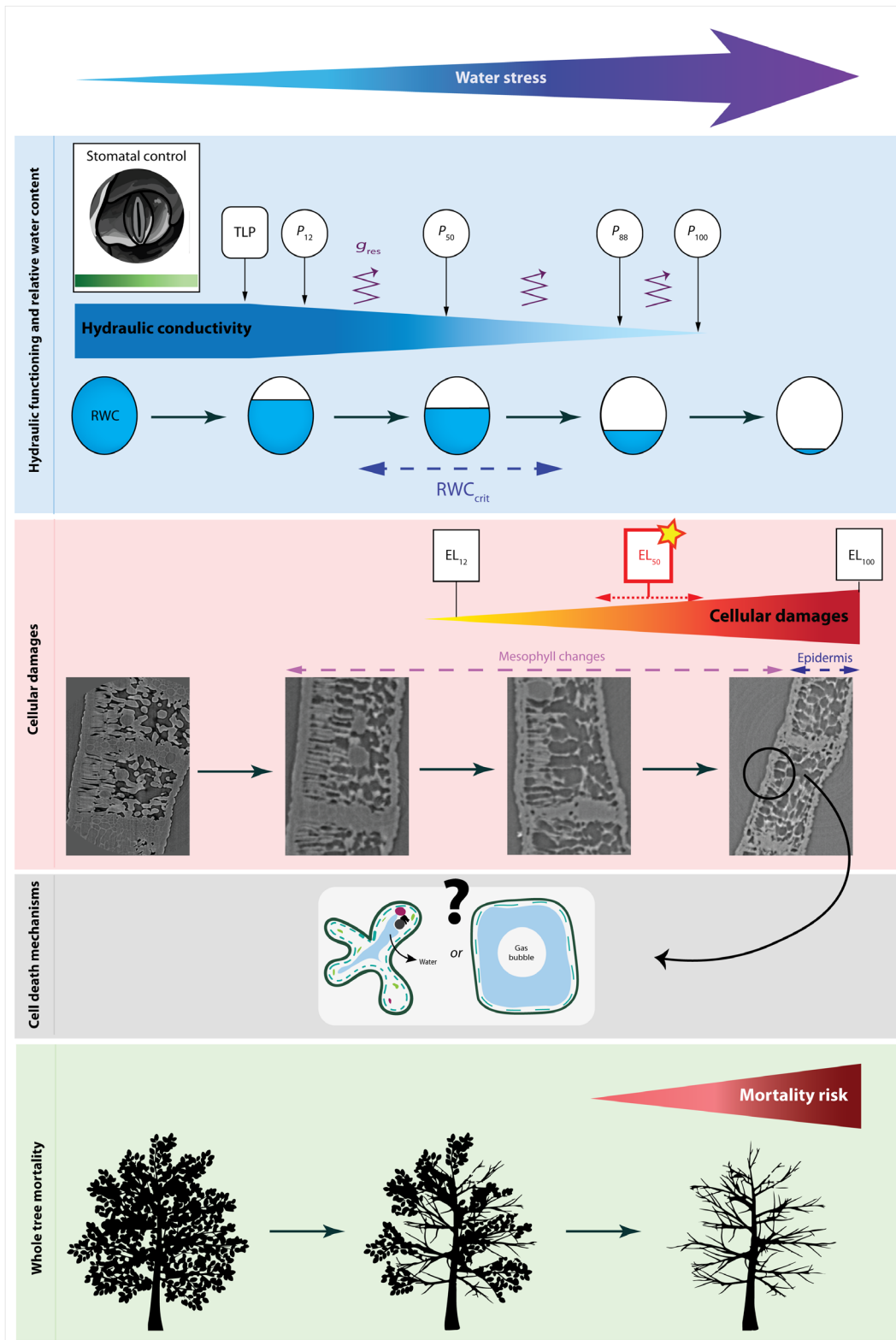


Fig. 8 Sequence of events leading trees to death. Star highlights EL_{50} (the RWC at which 50% of cell damage is encountered) as a potential indicator for cellular resistance to drought. Jagged arrows symbolise residual water losses. Black solid arrows represent the sequence of events. Dashed arrows indicate the range where the events can occur.

dehydration, our results provide evidence that xylem HF precedes the onset of cell mortality in woody species. We describe a critical RWC value, an important dehydration threshold, below which living cells start to suffer damage from drought, and that corresponds to a certain degree of embolism occurrence. This critical RWC value varies across species with contrasted cavitation resistance. Despite micro-CT analyses showing a clear correlation between cell structural changes and mortality at the mesophyll level along dehydration, whether cells are dying because of cell cavitation or cytorrhysis remains unresolved. This approach represents a first step in deciphering how hydraulic dysfunction could induce damage to key living tissues as, for example the meristems, and thus ultimately determine trees' point of death under drought conditions.


Acknowledgements

This research was supported by La Région Auvergne-Rhône-Alpes 'Pack Ambition International 2020' through the project 'ThirsTree' 20-006175-01, 20-006175-02 and the Agence Nationale de la Recherche, grant/award no. ANR-18-CE20-0005, 'Hydrauleaks'.

Author contributions

MM and JMT-R conceived and designed the experiment. MM was responsible for running the measurements and carrying out the data analysis. AK and SD supervised the setting up of the micro-CT scans. MM, JMT-R, ST, MAA, CMR-D, RB, SD and HC ran the micro-CT scans. MM, JMT-R, HC and ST interpreted and discussed the results. MM wrote the first manuscript draft. All authors assisted substantially with manuscript development.

ORCID

Mutez A. Ahmed  <https://orcid.org/0000-0002-7402-1571>
 Régis Burlett  <https://orcid.org/0000-0001-8289-5757>
 Hervé Cochard  <https://orcid.org/0000-0002-2727-7072>
 Sylvain Delzon  <https://orcid.org/0000-0003-3442-1711>
 Marylou Mantova  <https://orcid.org/0000-0003-4445-3100>
 Celia M. Rodriguez-Dominguez  <https://orcid.org/0000-0003-2352-0829>
 José M. Torres-Ruiz  <https://orcid.org/0000-0003-1367-7056>
 Santiago Trueba  <https://orcid.org/0000-0001-8218-957X>

Data availability

All data are available upon request.

References

- Abate E, Nardini A, Petruzzellis F, Trifil P. 2021. Too dry to survive: leaf hydraulic failure in two *Salvia* species can be predicted on the basis of water content. *Plant Physiology and Biochemistry* 166: 215–224.
- Adams HD, Zeppel MJB, Anderegg WRL, Hartmann H, Landhäusser SM, Tissue DT, Huxman TE, Hudson PJ, Franz TE, Allen CD *et al.* 2017. A multi-species synthesis of physiological mechanisms in drought-induced tree mortality. *Nature Ecology and Evolution* 1: 1285–1291.
- Allen CD, Macalady AK, Chenchouni H, Bachelet D, McDowell N, Venetier M, Kitzberger T, Rigling A, Breshears DD, Hogg EH *et al.* 2010. A global overview of drought and heat-induced tree mortality reveals emerging climate change risks for forests. *Forest Ecology and Management* 259: 660–684.
- Anderegg WRL, Flint A, Huang CY, Flint L, Berry JA, Davis FW, Sperry JS, Field CB. 2015. Tree mortality predicted from drought-induced vascular damage. *Nature Geoscience* 8: 367–371.
- Barigah TS, Charrier O, Douris M, Bonhomme M, Herbette S, Améglio T, Fichot R, Brignolas F, Cochard H. 2013. Water stress-induced xylem hydraulic failure is a causal factor of tree mortality in beech and poplar. *Annals of Botany* 112: 1431–1437.
- Barrs H, Weatherley PE. 1962. A re-examination of the relative turgidity techniques for estimating water deficits in leaves. *Australian Journal of Biological Sciences* 15: 413–428.
- Bartlett MK, Klein T, Jansen S, Choat B, Sack L. 2016. The correlations and sequence of plant stomatal, hydraulic, and wilting responses to drought. *Proceedings of the National Academy of Sciences, USA* 113: 13098–13103.
- Bartlett MK, Scaffoni C, Sack L. 2012. The determinants of leaf turgor loss point and prediction of drought tolerance of species and biomes: a global meta-analysis. *Ecology Letters* 15: 393–405.
- Billon LM, Blackman CJ, Cochard H, Badel E, Hitmi A, Cartailleur J, Souchal R, Torres-Ruiz JM. 2020. The DroughtBox: a new tool for phenotyping residual branch conductance and its temperature dependence during drought. *Plant, Cell & Environment* 43: 1584–1594.
- Bourbia I, Pritzkow C, Brodribb TJ. 2021. Herb and conifer roots show similar high sensitivity to water deficit. *Plant Physiology* 186: 1908–1918.
- Brodribb T, Brodersen CR, Carriqui M, Tonet V, Rodríguez Domínguez C, McAdam S. 2021. Linking xylem network failure with leaf tissue death. *New Phytologist* 232: 68–79.
- Brodribb TJ, Carriqui M, Delzon S, Lucani C. 2017. Optical measurement of stem xylem vulnerability. *Plant Physiology* 174: 2054–2061.
- Brodribb TJ, Cochard H. 2009. Hydraulic failure defines the recovery and point of death in water-stressed conifers. *Plant Physiology* 149: 575–584.
- Brodribb TJ, Holbrook NM, Edwards EJ, Gutiérrez MV. 2003. Relations between stomatal closure, leaf turgor and xylem vulnerability in eight tropical dry forest trees. *Plant, Cell & Environment* 26: 443–450.
- Brodribb TJ, Powers J, Cochard H, Choat B. 2020. Hanging by a thread? Forests and drought. *Science* 368: 261–266.
- Brodribb TJ, Skelton RP, McAdam SAM, Bienaimé D, Lucani CJ, Marmottant P. 2016. Visual quantification of embolism reveals leaf vulnerability to hydraulic failure. *New Phytologist* 209: 1403–1409.
- Chaturvedi AK, Patel MK, Mishra A, Tiwari V, Jha B. 2014. The SbMT-2 gene from a halophyte confers abiotic stress tolerance and modulates ROS scavenging in transgenic tobacco. *PLoS ONE* 9: e111379.
- Choat B, Jansen S, Brodribb TJ, Cochard H, Delzon S, Bhaskar R, Bucci SJ, Feild TS, Gleason SM, Hacke UG *et al.* 2012. Global convergence in the vulnerability of forests to drought. *Nature* 491: 752–755.
- Creek D, Lamarque LJ, Torres-Ruiz JM, Parise C, Burlett R, Tissue DT, Delzon S. 2020. Xylem embolism in leaves does not occur with open stomata: evidence from direct observations using the optical visualization technique. *Journal of Experimental Botany* 71: 1151–1159.
- Duursma R, Choat B. 2017. FITPLC – an R package to fit hydraulic vulnerability curves. *Journal of Plant Hydraulics* 4: e002.
- Guadagno CR, Ewers BE, Speckman HN, Aston TL, Huhn BJ, DeVore SB, Ladwig JT, Strawn RN, Weinig C. 2017. Dead or alive? Using membrane failure and chlorophyll fluorescence to predict mortality from drought. *Plant Physiology* 175: 223–234.
- Hammond WM, Yu KL, Wilson LA, Will RE, Anderegg WRL, Adams HD. 2019. Dead or dying? Quantifying the point of no return from hydraulic failure in drought-induced tree mortality. *New Phytologist* 223: 1834–1843.
- IPCC. 2022. Chapter 4: Water. In: Pörtner H-O, Roberts DC, Adams H, Adler C, Aldunce P, Ali E, Begum RA, Betts R, Kerr RB, Biesbroek R *et al.*, eds.

- Climate change 2022: impacts, adaptation and vulnerability summary for policymakers*. Cambridge, UK: Cambridge University Press.
- Joardder MUH, Brown RJ, Kumar C, Karim MA. 2015. Effect of cell wall properties on porosity and shrinkage of dried apple. *International Journal of Food Properties* 18: 2327–2337.
- John GP, Henry C, Sack L. 2018. Leaf rehydration capacity: associations with other indices of drought tolerance and environment. *Plant, Cell & Environment* 41: 2638–2653.
- Johnson KM, Jordan GJ, Brodribb TJ. 2018. Wheat leaves embolized by water stress do not recover function upon rewatering. *Plant, Cell & Environment* 41: 2704–2714.
- Johnson KM, Lucani C, Brodribb TJ. 2022. *In vivo* monitoring of drought-induced embolism in *Callitris rhomboidea* trees reveals wide variation in branchlet vulnerability and high resistance to tissue death. *New Phytologist* 233: 207–218.
- King M, Ludford PM. 1983. Chilling injury and electrolyte leakage in fruit of different tomato cultivars. *Journal of the American Society for Horticultural Science* 108: 74–77.
- Lamacque L, Charrier G, dos Santos Farnese F, Lemaire B, Ameglio T, Herbette S. 2020. Drought-induced mortality: branch diameter variation reveals a point of no recovery in lavender species. *Plant Physiology* 183: 1638–1649.
- Lemaire C, Blackman CJ, Cochard H, Menezes-Silva PE, Torres-Ruiz JM, Herbette S. 2021. Acclimation of hydraulic and morphological traits to water deficit delays hydraulic failure during simulated drought in poplar. *Tree Physiology* 41: 2008–2021.
- Mantova M, Herbette S, Cochard H, Torres-Ruiz JM. 2022. Hydraulic failure and tree mortality: from correlation to causation. *Trends in Plant Science* 27: 335–345.
- Mantova M, Menezes-Silva PE, Badel E, Cochard H, Torres-Ruiz JM. 2021. The interplay of hydraulic failure and cell vitality explains tree capacity to recover from drought. *Physiologia Plantarum* 172: 247–257.
- Martinez-Vilalta J, Anderegg WRL, Sapes G, Sala A. 2019. Greater focus on water pools may improve our ability to understand and anticipate drought-induced mortality in plants. *New Phytologist* 223: 22–32.
- McDowell N, Pockman WT, Allen CD, Breashears DD, Cobb N, Kolb T, Plaut J, Sperry J, West A, Williams DG *et al.* 2008. Mechanisms of plants survival and mortality during drought: why do some plants survive while others succumb to drought? *New Phytologist* 178: 719–739.
- McDowell NG, Sapes G, Pivovarov A, Adams HD, Allen CD, Anderegg WRL, Arend M, Breashears DD, Brodribb T, Choat B *et al.* 2022. Mechanisms of woody-plant mortality under rising drought, CO₂ and vapour pressure deficit. *Nature Reviews Earth & Environment* 3: 294–308.
- Meinzer FC, Johnson DM, Lachenbruch B, McCulloh KA, Woodruff DR. 2009. Xylem hydraulic safety margins in woody plants: coordination of stomatal control of xylem tension with hydraulic capacitance. *Functional Ecology* 23: 922–930.
- Mirone A, Brun E, Gouillart E, Tafforeau P, Kieffer J. 2014. The PyHST2 hybrid distributed code for high speed tomographic reconstruction with iterative reconstruction and *a priori* knowledge capabilities. *Nuclear Instruments and Methods in Physics Research, Section B: Beam Interactions with Materials and Atoms* 324: 41–48.
- Momayyezi M, Borsuk AM, Brodersen CR, Gilbert ME, Thérout-Rancourt G, Kluepfel DA, McElrone AJ. 2022. Desiccation of the leaf mesophyll and its implications for CO₂ diffusion and light processing. *Plant, Cell & Environment* 45: 1362–1381.
- Moore JP, Vitré-Gibouin M, Farrant JM, Driouich A. 2008. Adaptations of higher plant cell walls to water loss: drought vs desiccation. *Physiologia Plantarum* 134: 237–245.
- Oertli JJ. 1986. The effect of cell size on cell collapse under negative turgor pressure. *Journal of Plant Physiology* 124: 365–370.
- Paganin D. 2006. *Coherent X-ray optics*. Oxford series on synchrotron radiation, vol. 6. Oxford, UK: Oxford University Press.
- Pammenter N, Vander Willigen C. 1998. A mathematical and statistical analysis of the curves illustrating vulnerability of xylem to cavitation. *Tree Physiology* 18: 589–593.
- Rajashekar CB, Lafta A. 1996. Cell-wall changes and cell tension in response to cold acclimation and exogenous abscisic acid in leaves and cell cultures. *Plant Physiology* 111: 605–612.
- Rodriguez-Dominguez CM, Forner A, Martorell S, Choat B, Lopez R, Peters JMR, Pfautsch S, Mayr S, Carins-Murphy MR, McAdam SAM *et al.* 2022. Leaf water potential measurements using the pressure chamber: synthetic testing of assumptions towards best practices for precision and accuracy. *Plant, Cell & Environment* 45: 2037–2061.
- Sack L, Dietrich EM, Streeter CM, Sánchez-Gómez D, Holbrook NM. 2008. Leaf palmate venation and vascular redundancy confer tolerance of hydraulic disruption. *Proceedings of the National Academy of Sciences, USA* 105: 1567–1572.
- Sack L, John GP, Buckley TN. 2018. ABA accumulation in dehydrating leaves is associated with decline in cell volume, not turgor pressure. *Plant Physiology* 176: 489–493.
- Sack L, Pasquet-Kok J, Bartlett M, Prometheus Protocols Contributors. 2010. *Leaf pressure–volume curve parameters, prometheus protocols*. [WWW document] URL <https://prometheusprotocols.net/funccion/water-relations/pressure-volume-curves/leaf-pressure-volume-curve-parameters/> [accessed 01 June 2021].
- Sakes A, van der Wiel M, Henselmans PWJ, van Leeuwen JL, Dodou D, Breedveld P. 2016. Shooting mechanisms in nature: a systematic review. *PLoS ONE* 11: e0158277.
- Salmon Y, Torres-Ruiz JM, Poyatos R, Martinez-Vilalta J, Meir P, Cochard H, Mencuccini M. 2015. Balancing the risks of hydraulic failure and carbon starvation: a twig scale analysis in declining Scots pine. *Plant, Cell & Environment* 38: 2575–2588.
- Sapes G, Roskilly B, Dobrowski S, Maneta M, Anderegg WRL, Martinez-Vilalta J, Sala A. 2019. Plant water content integrates hydraulics and carbon depletion to predict drought-induced seedling mortality. *Tree Physiology* 39: 1300–1312.
- Schindelin J, Arganda-Carreras I, Frise E, Kaynig V, Longair M, Pietzsch T, Preibisch S, Rueden C, Saalfeld S, Schmid B *et al.* 2012. Fiji: an open-source platform for biological-image analysis. *Nature Methods* 9: 676–682.
- Scoffoni C, Vuong C, Diep S, Cochard H, Sack L. 2014. Leaf shrinkage with dehydration: coordination with hydraulic vulnerability and drought tolerance. *Plant Physiology* 164: 1772–1788.
- Sperry JS, Love DM. 2015. What plant hydraulics can tell us about responses to climate-change droughts. *New Phytologist* 207: 14–27.
- Sutinen M-L, Palta JP, Reich PB. 1992. Seasonal differences in freezing stress resistance of needles of *Pinus nigra* and *Pinus resinosa*: evaluation of the electrolyte leakage method. *Tree Physiology* 11: 241–254.
- Taiz L, Zeiger E. 2006. *Plant physiology*. Sunderland, MA, USA: Sinauer Associates, 46–47.
- Torres-Ruiz JM, Cochard H, Choat B, Jansen S, López R, Tomášková I, Padilla-Díaz CM, Badel E, Burlett R, King A *et al.* 2017. Xylem resistance to embolism: presenting a simple diagnostic test for the open vessel artefact. *New Phytologist* 215: 489–499.
- Trueba S, Pan R, Scoffoni C, John GP, Davis SD, Sack L. 2019. Thresholds for leaf damage due to dehydration: declines of hydraulic function, stomatal conductance and cellular integrity precede those for photochemistry. *New Phytologist* 223: 134–149.
- Urli M, Porté AJ, Cochard H, Guengant Y, Burlett R, Delzon S. 2013. Xylem embolism threshold for catastrophic hydraulic failure in angiosperm trees. *Tree Physiology* 33: 672–683.
- Vilagrosa A, Morales F, Abadía A, Bellot J, Cochard H, Gil-Pelegrin E. 2010. Are symplast tolerance to intense drought conditions and xylem vulnerability to cavitation coordinated? An integrated analysis of photosynthetic, hydraulic and leaf level processes in two Mediterranean drought-resistant species. *Environmental and Experimental Botany* 69: 233–242.
- Wang C-R, Yang A-F, Yue G-D, Gao Q, Yin H-Y, Zhang J-R. 2008. Enhanced expression of phospholipase C 1 (ZmPLC1) improves drought tolerance in transgenic maize. *Planta* 227: 1127–1140.
- Zhang MIN, Willison JHM. 1987. An improved conductivity method for the measurement of frost hardiness. *Canadian Journal of Botany* 65: 710–715.
- Zhu JK. 2016. Abiotic stress signaling and responses in plants. *Cell* 167: 313–324.

Supporting Information

Additional Supporting Information may be found online in the Supporting Information section at the end of the article.

Fig. S1 Graphs representing the loss in rehydration capacity when leaf relative water content decreases below 30% for *Eucalyptus viminalis* and below 25% for *Laurus nobilis*.

Fig. S2 Pressure–volume curves examples for *Populus tremula* × *alba*, *Eucalyptus viminalis* and *Laurus nobilis*.

Fig. S3 Vulnerability curves to cavitation for *Populus tremula* × *alba*, *Eucalyptus viminalis* and *Laurus nobilis*.

Fig. S4 Damages at the epidermis level after full embolization of the xylem vessels for *Populus tremula* × *alba* and *Eucalyptus viminalis* observed with synchrotron-based X-ray micro-CT.

Please note: Wiley is not responsible for the content or functionality of any Supporting Information supplied by the authors. Any queries (other than missing material) should be directed to the *New Phytologist* Central Office.